RESEARCH PAPER

Stabilization of aqueous nanoscale zerovalent iron dispersions by anionic polyelectrolytes: adsorbed anionic polyelectrolyte layer properties and their effect on aggregation and sedimentation

**Tanapon Phenrat · Navid Saleh · Kevin Sirk · Hye-Jin Kim ·
Robert D. Tilton · Gregory V. Lowry**

Abstract Nanoscale zerovalent iron (NZVI) particles are 5–40 nm sized Fe^0/Fe-oxide particles that rapidly transform many environmental contaminants to benign products and are a promising in situ remediation agent. Rapid aggregation and limited mobility in water-saturated porous media limits the ability to deliver NZVI dispersions in the subsurface. This study prepares stable NZVI dispersions through physisorption of commercially available anionic polyelectrolytes, characterizes the adsorbed polymer layer, and correlates the polymer coating properties with the ability to prevent rapid aggregation and sedimentation of NZVI dispersions. Poly(styrene sulfonate) with molecular weights of 70 k and 1,000 k g/mol (PSS70K and PSS1M), carboxymethyl cellulose with molecular weights of 90 k and 700 k g/mol (CMC90K and CMC700K), and polyaspartate with molecular weights of 2.5 k and 10 k g/mol (PAP2.5K and 10K) were compared. Particle size distributions were determined by dynamic light scattering during aggregation. The order of effectiveness to prevent rapid aggregation and stabilize the dispersions was PSS70K(83%) > ≈PAP10K(82%) > PAP2.5K(72%) > CMC700K(52%), where stability is defined operationally as the volume percent of particles that do not aggregate after 1 h. CMC90K and PSS1M could not stabilize RNIP relative to bare RNIP. A similar trend was observed for their ability to prevent sedimentation, with 40, 34, 32, 20, and 5 wt%, of the PSS70K, PAP10K, PAP2.5K, CMC700K, and CMC90K modified NZVI remaining suspended after 7 h of quiescent settling, respectively. The stable fractions with respect to both aggregation and sedimentation correlate well with the adsorbed polyelectrolyte mass and thickness of the adsorbed polyelectrolyte layers as determined by Oshima's soft particle theory. A fraction of the particles cannot be stabilized by any modifier and rapidly agglomerates to micron sized aggregates, as is also observed for unmodified NZVI. This non-dispersible fraction is attributed to strong magnetic attractions among the larger particles present in the polydisperse NZVI slurry, as the magnetic attractive forces increase as r^6.

T. Phenrat · N. Saleh · H.-J. Kim · G. V. Lowry (✉)
Department of Civil & Environmental Engineering,
Carnegie Mellon University, 5000 Forbes Ave.,
119 Porter Hall, Pittsburgh, PA 15213-3890, USA
e-mail: glowry@cmu.edu

K. Sirk · R. D. Tilton · G. V. Lowry
Department of Chemical Engineering, Carnegie Mellon
University, Pittsburgh, PA 15213-3890, USA

R. D. Tilton
Department of Biomedical Engineering, Carnegie Mellon
University, Pittsburgh, PA 15213-3890, USA

Groundwater remediation ·
Nanoparticle environmental fate and transport

Abbreviations

|	
NZVI	Nanoscale zerovalent iron
PSS	Poly(styrene sulfonate)
CMC	Carboxymethyl cellulose
PAP	Polyaspartate
DLVO	Derjaguin–Landau–Verwey–Overbeek
RNIP	Reactive nano-scale iron particles
DLS	Dynamic light scattering

Introduction

The high specific surface area and resulting high reactivity of nanoscale zerovalent iron (NZVI) makes it a promising and flexible technology for in situ remediation of groundwater contaminants that are amenable to reduction by Fe^0, e.g. chlorinated organic contaminants and heavy metals (Kanel et al. 2007; Liu and Lowry 2006; Liu et al. 2005; Ponder et al. 2000; Wu et al. 2005; Xu et al. 2005; Zhang 2003). Early field demonstrations indicate NZVI as a promising in situ groundwater remediation technology (Elliott and Zhang 2001; Henn and Waddill 2006), however, high reactivity alone is not sufficient to make NZVI a good in situ remediation agent. NZVI particles must also be readily dispersible in water such that they can migrate through water-saturated porous media to the contaminated area. Thus, for the purpose of in situ environmental remediation, colloidal stability of an aqueous NZVI dispersion is a critical property.

Colloidal stability is defined operationally as the ability of a particle dispersion to resist aggregation for a specified time (Hiemenz and Rajagopalan 1997; Strenge 1993). Colloidal stability requires an energy barrier of at least several kT in the interparticle interaction potential. According to the DLVO theory, the net interaction energy between particles is the sum of van der Waals attraction and electrostatic double layer repulsion and depends on the size, Hamaker constant, and surface potential of the particles, and on the solution ionic strength (Elimelech et al. 1995; Evans and Wennerstrom 1999;

Hiemenz and Rajagopalan 1997). NZVI exposed to water acquires an oxide shell, resulting in Fe^0/Fe-oxide core/shell particles. Reactive nano-scale iron particles (RNIP) manufactured by Toda Kogyo, Japan, specifically for in situ groundwater remediation, have a Fe^0 core and a primarily magnetite (Fe_3O_4) shell (Liu et al. 2005; Nurmi et al. 2005), both of which are magnetic (McCurrie 1994; Rosenweig 1985). We recently reported the rapid aggregation and gelation of chain-like aggregates in aqueous bare (unmodified) RNIP dispersions. The rapid aggregation resulted from the magnetic attractive force between particles due to their intrinsic magnetic moments (Phenrat et al. 2007). Gelation of the chain-like aggregates not only increases the size of NZVI clusters being transported, which might cause pore plugging during the intended groundwater application (Phenrat et al. 2007; Saleh et al. 2007), but also enhances gravitational sedimentation (Allain and Cloitre 1993; Phenrat et al. 2007) which might promote particle deposition (Elimelech et al. 1995). For this reason, particle modification to introduce long range repulsive forces that overcome the attractive forces is required to enhance NZVI colloidal stability and thus its mobility in groundwater.

Surface modification by physisorption of charged macromolecules has received a great deal of attention (Goddard and Vincent 1984; Sato and Ruch 1980), especially in industrial applications (Duro et al. 1999), as a mean to enhance colloidal stability of both magnetic (Viota et al. 2005; Williams et al. 2006) and non-magnetic dispersions (Kim and Sigmund 2004; Singh et al. 2005). Adsorption of charged macromolecules onto the particle surface is governed by the molecular weight, ionization and charge density of the macromolecule, the charge density and polarity of the solid surface, the solvent quality, and ionic strength (Fleer et al. 1993; Holmberg et al. 2003). The mass adsorbed and the configuration of the adsorbed layer is dictated by a balance between electrostatic attraction to the surface and repulsions among neighboring ionized monomer units, a loss of chain entropy upon adsorption, and also nonspecific dipolar interactions between the macromolecule, the solvent and the surface (Fleer et al. 1993; Holmberg et al. 2003).

Adsorbed layers of charged macromolecules provide the particles with electrosteric repulsive forces, i.e. a combination of steric repulsion and electrostatic
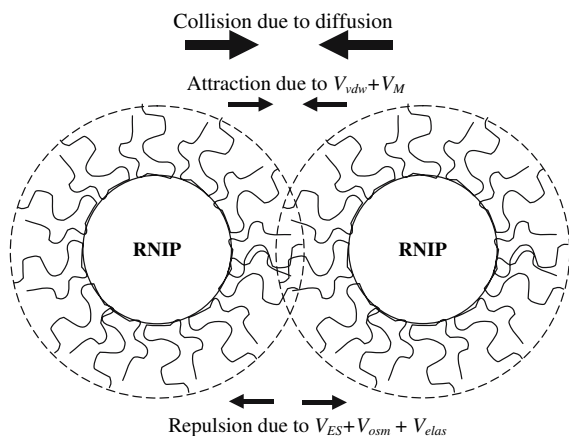
Fig. 1 Schematic representation of the forces acting on electrosterically stabilized polyelectrolyte-modified RNIP including van der Waals attraction (V_{vdW}), electrostatic double layer repulsion (V_{ES}), magnetic attraction (V_M), osmotic repulsion (V_{osm}), and elastic-steric repulsion (V_{elas})

repulsion (Fig. 1) (Fritz et al. 2002; Napper 1983; Romero-Cano et al. 2001). Between a pair of particles, the steric repulsion consists of two contributions: osmotic repulsion (V_{osm}) and elastic-steric repulsion (V_{elas}). The range and magnitude of the electrosteric repulsion between a pair of particles depends on the surface concentration, extension and charge density of the adsorbed polyelectrolyte layer.

Our recent studies have demonstrated the enhancement of NZVI colloidal stability (Saleh et al. 2005) and mobility through saturated porous media (Saleh et al. 2007) by adsorbing a novel series of triblock copolymers to the NZVI surface. However, these experimental triblock copolymers are synthesized in small quantities and have not yet been scaled up for large scale field application. Therefore, one objective of this study is to evaluate the ability of inexpensive and commercially available anionic polyelectrolytes, including polystyrene sulfonate (sodium salt) (PSS), carboxymethyl cellulose (sodium salt) (CMC), and polyaspartate (sodium salt) (PAP), to stabilize NZVI dispersions against aggregation and sedimentation. The PAP monomer unit is aspartate, one of the 20 natural amino acid building blocks of proteins, making PAP of interest as potentially an environmentally benign modifier. A modified biopolymer, CMC may also be a potentially benign modifier. The use of anionic polyelectrolytes is particularly relevant to groundwater mobility, since most mineral and natural organic matter surfaces encountered in
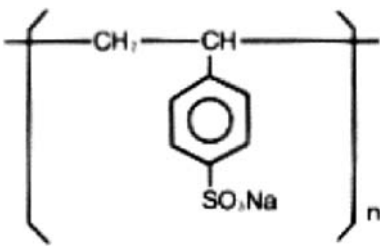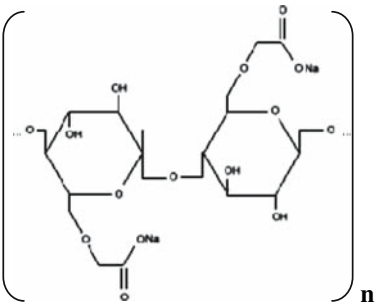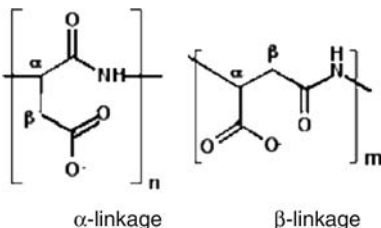
groundwater are negatively charged. Thus, the coating must also provide electrostatic repulsion from these surfaces in order to minimize adhesion and filtration. The second objective is to characterize the properties of the absorbed polyelectrolyte layers, including adsorbed mass and layer thickness, and correlate these properties with the ability of each modifier to stabilize the NZVI dispersions. Therefore, we measure an adsorption isotherm for each polyelectrolyte on NZVI and characterize each adsorbed polyelectrolyte layer in terms of electrical potential, thickness, and a softness parameter that relates to solvent drainage through the layer (Ohshima 1995a). Although dynamic light scattering (DLS) is sometimes used to estimate the thickness of polymer layers adsorbed on colloidal particles, the RNIP in this study is far too polydisperse to allow an accurate thickness determination by DLS. Therefore, we used Ohshima's approach, which is not very sensitive to particle polydispersity for the size of particles (5 nm to 40 nm) and measured layer thicknesses used here (see Appendix). Finally, extended DLVO theory that includes both magnetic attraction and steric repulsions in addition to the usual van der Waals and electrostatic double layer forces is used to semiquantitatively support the experimentally observed effects of each adsorbed polyelectrolyte on the aggregation and sedimentation of NZVI.

Experimental

Nanoscale zerovalent iron particles

Reactive nanoscale iron particles (RNIP), commercially available reactive Fe^0/Fe_3O_4 core-shell NZVI particles, were obtained from Toda Kogyo, Japan. The physical and chemical properties of RNIP were reported previously (Liu et al. 2005; Nurmi et al. 2005; Phenrat et al. 2007). RNIP consists of a polydisperse suspension of irregularly shaped particles, with primary particles ranging in size from 5 nm to 40 nm with a median radius of ~ 20 nm. Prior to use, RNIP had been stored as an aqueous slurry (pH 10.6) at approximately 300 g/L under anaerobic conditions in a glove box for 6 months. From this slurry, an aqueous stock dispersion (10 mL at 120 g/L) was prepared in 1 mM $NaHCO_3$ using an ultrasonic probe (550 sonic dismembrator, Fisher Scientific,

Table 1 Chemical properties and structures of polyelectrolyte surface modifiers

Code	Polymer name/category	Average monomer M_W (g/mol)	M_w^a (kg/mol)	D_P^b	Structure
PSS70K	Poly(styrene sulfonate)/ strong anionic polyelectrolyte	206	70	340	
PSS1M		206	1,000	4,850	
CMC90K	Carboxymethylcellulose/ weak anionic polysaccharide	263	90	342	
CMC700K		263	700	2,661	
PAP2.5K	Polyaspartate/weak anionic polypeptide	156	2–3	16	
PAP10K		156	10	64	

[a] Polyelectrolyte molecular weight as specified by the manufacturer

[b] Average degree of polymerization, D_p, is estimated by dividing M_w of a polymer with the average molecular weight of a monomer unit

Howell, NJ) at power level 3 for 30 min to break aggregates that formed during storage. This sonicated stock dispersion was then diluted again with 1 mM NaHCO$_3$ to ∼6 g/L. The specific surface area of RNIP was determined by the BET method to be 15 ± 0.5 m^2/g.
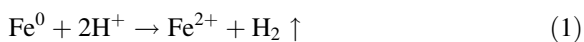
Polyelectrolytes

Poly(styrene sulfonate) and carboxymethylcellulose were from Aldrich (St. Louis, MO). Polyaspartate at molecular weight of 2–3 and 10 kg/mol was

from Lanxess (Pittsburgh, PA) and NanoChem Solutions Inc. (Bedford Park, IL), respectively. All the polyelectrolytes are negatively charged with sodium as a counterion. Table 1 summarizes the properties and structures of these modifiers. PSS, PAP, and CMC stock solutions were prepared at 4 g/L in 1 mM NaHCO$_3$. PSS and PAP were agitated using an orbital shaker at 25 °C for 12 h prior to the adsorption study. CMC stock solutions were agitated using an orbital shaker at 25 °C for 1 h and refrigerated overnight to ensure complete hydration and dissolution.

Adsorption isotherms

The adsorption isotherms of the polyelectrolytes on RNIP were measured by the solution depletion method with the following conditions: All suspensions contained 3 g/L RNIP and 1 mM NaHCO$_3$. Polyelectrolyte stock solution aliquots were added to provide equilibrium polyelectrolyte concentrations ranging from 5 to 1,000 mg/L. The pH of the mixtures was from 9.5 to 10.5 due to the oxidation of Fe^0 in the particles and subsequent production of OH$^-$ (Liu and Lowry 2006). The isoelectric point of bare RNIP is pH 6.3. Therefore, bare RNIP is negatively charged in this study. The samples were mixed at 25°C for 48 h using an end-over-end rotator at 30 rpm. Afterward, they were centrifuged at 27,500 rpm for 80 min (Sorvall® Ultracentrifuge OTD65B) to separate the particles from the supernatant. The equilibrium concentration of non-adsorbed PSS in the supernatant was measured by the absorbance at 225 nm (extinction coefficient = 0.04 L mg^{-1} cm^{-1}) using a UV–vis spectrophotometer (Varian, Palo Alto, CA). The equilibrium concentration of PAP and CMC were measured using a total organic carbon analyzer (OI Analytical). The adsorbed mass was calculated from the difference between the initial and equilibrium concentrations. Each isotherm point was measured from duplicate samples. Isotherms are plotted using the average sorbed mass and equilibrium concentration and multi-directional error bars showing the standard deviation of the measurements.

The total iron (Fe^0 + Fe-oxides) in each reactor was determined by atomic absorption spectrometry (AA) after acid digestion in concentrated HCl (trace metal grade). The Fe^0 content of RNIP was also determined (separately from total iron) by acid digestion in a closed container with headspace. H$_2$ produced from the oxidation of Fe^0 in RNIP by H$^+$ is used to quantify the Fe^0 content of the particles (Eq. 1) (Liu et al. 2005). The RNIP concentration was calculated assuming a Fe^0(core)/Fe$_3$O$_4$(shell) morphology, and using the measured Fe^0 content, α (Eqs. 2–3). The factor 1.38 in Eq. 3 is to convert the mass of iron (Fe) to magnetite (Fe$_3$O$_4$).

$$Fe^0 + 2H^+ \rightarrow Fe^{2+} + H_2 \uparrow \tag{1}$$

$$[Fe]_{total} = [Fe]_{Fe_3O_4} + [Fe]_{Fe^0} \tag{2}$$

$$[RNIP] = 1.38(1 - \alpha)[Fe]_{total} + \alpha[Fe]_{total} \tag{3}$$

Adsorbed polyelectrolyte layer characterization, aggregation, and sedimentation

Adsorbed polyelectrolyte layer characterization measurements, aggregation, and sedimentation were conducted on samples prepared with 3 g/L RNIP and 1 g/L polyelectrolyte in 1 mM NaHCO$_3$. After equilibration, the dispersions were centrifuged at 27,500 rpm for 80 min, washed to remove free polymer from solution, and re-suspended in 1 mM NaHCO$_3$. This process was repeated three times followed by ultrasonication for 10 min prior to measuring aggregation, sedimentation, or electrophoretic mobility as described next.

Adsorbed polyelectrolyte layer characterization

The adsorbed polyelectrolyte layer was characterized using electrophoretic mobility (EM) measurements and Ohshima's soft particle theory. Polyelectrolyte-modified NZVI particles are soft particles, i.e. the charge is distributed over a finite layer at the surface of the particle and thus cannot be treated as a sharp surface of charge, so Ohshima's soft particle theory was used to determine their electrical double-layer characteristics. Ohshima's approach (Fig. 2) assumes that the electrical potential around a polyelectrolyte adsorbed onto a solid surface consists of two separate electrical potentials in two different regions: the Donnan potential (ψ_{DON}) inside the adsorbed layer of thickness d, and the surface potential (ψ_0) at the boundary between the adsorbed layer and the surrounding solution (Ohshima 1995a). This model assumes that the polyelectrolyte segments act as resistance centers (Fig. 2c) that exert frictional forces on the liquid given by $-\gamma u$, where γ is the friction coefficient and u is the local liquid velocity inside the polyelectrolyte layer. It is assumed that the ionized groups each contribute a charge Ze (Z, valence of the ionized groups on the polyelectrolyte, which is –1 for all polyelectrolytes in this study; e, the electron charge), that they are uniformly

Fig. 2 (**a**) Conceptual model of surface modified RNIP based on Ohshima's soft particle theory; a is the particle radius, d is the layer thickness of the extended polyelectrolyte layer, and $1/\kappa$ is the Debye length. (**b**) Ion distribution inside and outside the negatively charged polyelectrolyte layer. (**c**) Schematic of each polyelectrolyte segment which is regarded as a series of resistance centers with radius a_p. (**d**) Assumed distribution of electrical potentials for an uncharged surface. (adapted from (Ohshima 1995b))
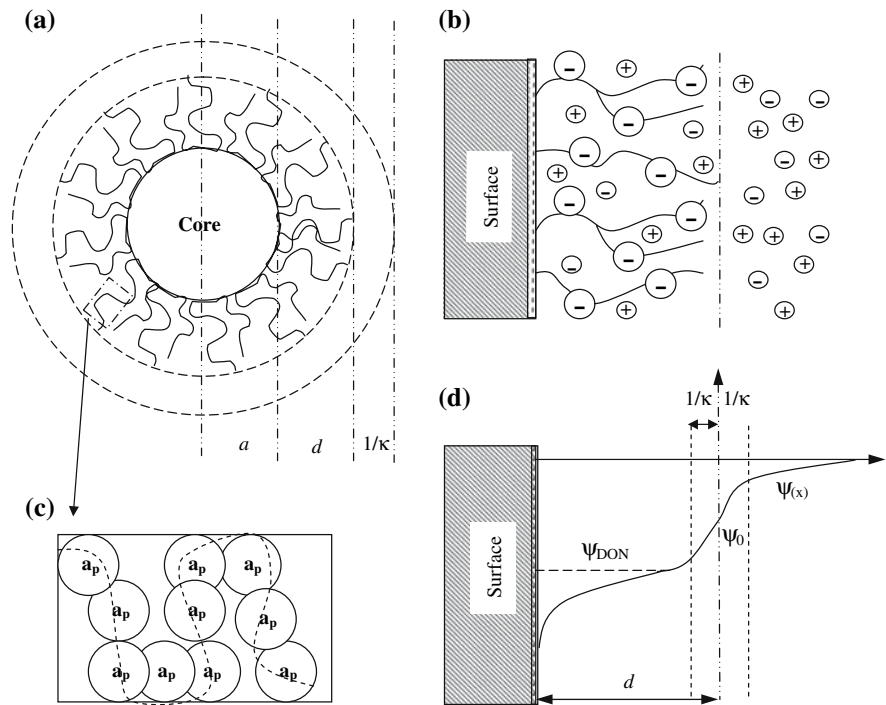
distributed within the adsorbed layer at a number density N (m^{-3}), and that the aqueous phase contains a symmetrical electrolyte of valence z, which is 1 for a 1:1 electrolyte such as NaCl used in this study, and bulk concentration n (m^{-3}). Considering the frictional force of the adsorbed layer in the Navier-Stokes equation, a modified expression for soft particles that relates their electrophoretic mobility u_e to the characteristics of a charged adsorbed layer on the charged surface of a particle of radius a is given by Eq. 4 (Nakamura et al. 1992; Ohshima 1994, 1995a; Ohshima et al. 1992),

$$u_e = \frac{\varepsilon}{\eta} \frac{\psi_0/\kappa_m + \psi_{DON}/\lambda}{1/\kappa_m + 1/\lambda} f\left(\frac{d}{a}\right) + \frac{ZeN}{\eta\lambda^2}$$
$$+ \frac{8\varepsilon k_B T}{\eta\lambda ze} \cdot \tanh\frac{ze\zeta}{4k_B T} \cdot \frac{e^{-\lambda d}/\lambda - e^{-\kappa_m d}/\kappa_m}{1/\lambda^2 - 1/\kappa_m^2} \quad (4)$$

where ε is the electric permittivity of the liquid medium, η is its viscosity, λ is a frictional parameter given by $(\gamma/\eta)^{1/2}$, and κ_m is the effective Debye-Hückel parameter of the surface hydrogel layer, which includes the contribution of the fixed charge ZeN (Ohshima 1995a). ζ is the apparent zeta potential of the bare particles calculated from EM measurements using Smoluchowski's formula. The function f(d/a) varies between 1 for a thin adsorbed layer

relative to radius of the core particle (a), to 2/3 for a thick layer. Equation 4 is valid when λd and $\kappa d > 1$ (Ohshima et al. 1992). The parameter $1/\lambda$ characterizes the softness of the polyelectrolyte layer; in the limit $1/\lambda \to 0$, the layer is rigid, and Eq. 4 tends to the classical Smoluchowski equation (Ohshima 1995a). The corresponding expressions for ψ_{DON}, ψ_0, f(d/a), and κ_m are given in Eqs. 5–8 (Nakamura et al. 1992; Ohshima 1994, 1995a; Ohshima et al. 1992),

$$\psi_{DON} = \frac{k_B T}{ze} \sinh^{-1}\left(\frac{ZN}{2zn}\right) \quad (5)$$

$$\psi_0 = \psi_{DON} - \frac{k_B T}{ze}\tanh\left(\frac{ze\psi_{DON}}{2k_B T}\right)$$
$$+ \frac{4k_B T}{ze}.e^{-\kappa_m d}\tanh\frac{ze\zeta}{4k_B T} \quad (6)$$

$$f\left(\frac{d}{a}\right) = \frac{2}{3}\left[1 + \frac{1}{2(1+d/a)^3}\right] \quad (7)$$

$$\kappa_m = \kappa\left[\cosh\left(\frac{ze\psi_{DON}}{k_B T}\right)\right]^{1/2} \quad (8)$$

where k_B is Boltzmann's constant, T is absolute temperature, and κ is the Debye-Hückel parameter of the solution. Use of the Ohshima method requires

data for the electrophoretic mobility for both the bare particles and for the polyelectrolyte-coated particles as a function of the bulk solution ionic strength.

The procedure for extracting the characteristics of the polyelectrolyte layer from EM data involves fitting Eq. 4, with terms defined as in Eqs. 5–8 to the experimental electrophoretic mobility vs. concentration of a symmetrical electrolyte (NaCl in this study) to obtain the best fit N, λ, and d (Ohshima 1994, 1995a, 1995b; Ohshima et al. 1992; Ramos-Tejada et al. 2003; Tsuneda et al. 2004; Viota et al. 2004, 2005). All other parameters in Eqs. 4–8 are fixed for a given salt concentration. A MATLAB (the Mathworks, Novi, MI) code employing iterative least squares minimization was used for this fitting the EM data (Fig. 4).

The EM was measured in 20 mg/L solutions of the washed, polyelectrolyte-coated RNIP for NaCl concentrations ranging from 1 to 61 mM (pH 8.5 ± 0.1) after 3 h of equilibration at the salt concentration used. It is assumed that the conformation of the adsorption layer is independent of the ionic strength over this range. The EM was measured in triplicate (25 °C) using a Malvern Zetasizer (Southborough, MA). The mean and standard deviation (σ) of the measured EM (u_e) for each polyelectrolyte-modified RNIP were calculated. Ohshima's model was then used to fit the mean u_e, mean $u_e + \sigma$, and mean $u_e - \sigma$ as a function of ionic strength to obtain three best-fit values of each fitting parameter ($1/\lambda$, N, and d). The average and standard deviation of the fitting parameters determined for the mean u_e, mean $u_e + \sigma$, and mean $u_e - \sigma$ was calculated and reported in Table 2. It should be noted that this procedure is not meant to convey the goodness of fit of the data, rather it is used

Table 2 Calculated surface excess, Γ_{max}, for each adsorbed polyelectrolytes

Sample	Γ_{max}		
	(mg/m²)	(10^{16} molecule/m²)	Average chain/particle
PSS70K	2.1 ± 0.3	1. 8 ± 0.2	74 ± 12
PSS1M	1.9 ± 0.2	0.1 ± 0.01	6 ± 0.7
CMC90K	1.0 ± 0.2	0.6 ± 0.1	33 ± 5
CMC700K	2.0 ± 0.1	0.2 ± 0.01	9 ± 0.4
PAP2.5K	2.3 ± 0.2	55.1 ± 5.6	2767 ± 279
PAP10K	2.2 ± 0.4	13.2 ± 2.1	665 ± 105

to bound the range of the magnitude of each parameter (Box et al. 1978; Mays and Hunt 2005).

Aggregation

Dynamic light scattering (Malvern Zetasizer, Southborough, MA) was used to monitor the time-dependent hydrodynamic diameter of aggregates during the early stage of aggregation (first 60 min). All measurements were conducted at 25 °C. Dilute samples (5, 30, and 60 mg/L) of the washed, polyelectrolyte-coated RNIP dispersions as well as the bare RNIP dispersions were used in order to avoid multiple scattering effects. The CONTIN algorithm was used to convert intensity autocorrelation functions to intensity-weighted particle hydrodynamic diameter distributions, assuming the Stokes-Einstein relationship for spherical particles.

To determine the fraction of the particle population that aggregates, comparisons between the intensity averaged DLS data and number averaged DLS data were made. Large particles scatter much more light than small particles because the scattering intensity is proportional to the sixth power of the particle diameter according to Rayleigh's approximation (Hiemenz and Rajagopalan 1997). Therefore, the intensity- averaged particle size distributions are particularly sensitive to aggregation even if only a small fraction of particles in the population aggregate. The number-averaged particle size distribution is less sensitive to aggregation. The intensity-weighted particle hydrodynamic diameter distributions were converted to volume- or number-weighted particle size distributions using the refractive index of the magnetite shell to represent the inhomogeneous refractive index of the Fe^0/Fe_3O_4 core-shell structure. The volume- and number-weighted particle size distributions of RNIP were insensitive to the choice of refractive index, i.e. using refractive index values for either Fe^0 ($n = 2.87 + 3.35i$) or Fe_3O_4 ($n = 2.42$) yielded similar particle size distributions (the difference is <5%).

It should be noted that although these experiments are conducted ex situ (i.e. in a DLS cuvette), the fundamental physics governing aggregation (i.e. all particle–particle interactions including van der Waals attraction, magnetic attraction, electrical double repulsion, and electrosteric repulsion) in these

experiments are also operable in porous media and the trends observed here should be useful for predicting aggregation behavior in porous media. Ex situ DLS aggregation experiments are a well-established method to understand nanoparticle (colloid) transport in porous media (Chen and Elimelech 2006; Dunphy Guzman et al. 2006; Wiesner et al. 2006).
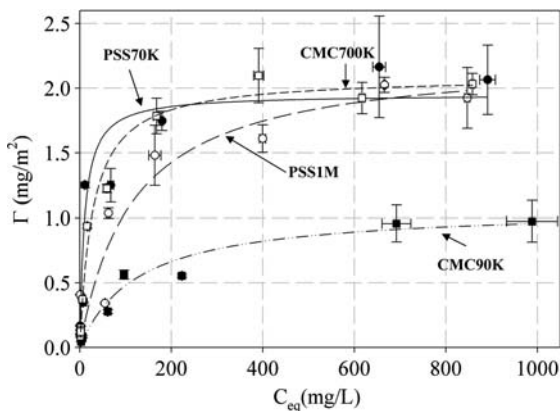
Sedimentation

The sedimentation of bare RNIP and the washed, polyelectrolyte-coated RNIP was determined for three different initial RNIP concentrations (100, 400, and 800 mg/L) by monitoring the optical absorbance at 800 nm as a function of time by UV–vis spectrophotometery (Varian, Palo Alto, CA). All measurements were made at 25 °C in duplicate.
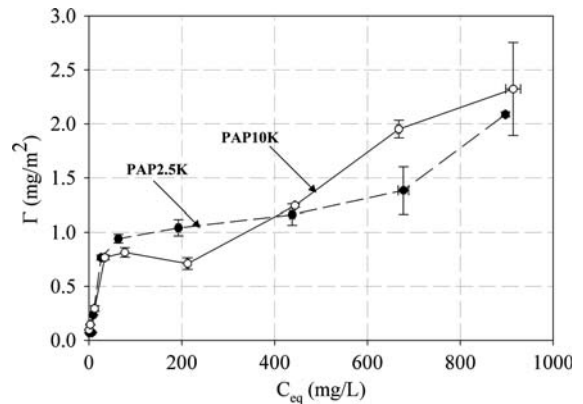
Results and discussion

Polyelectrolyte adsorption to RNIP

Adsorption isotherms for PSS and CMC are provided in Fig. 3, and for PAP in Fig. 4. The maximum attained surface excess concentration, Γ_{max} (mg/m^2), is calculated for each polyelectrolyte using the measured BET surface area (15 m^2/g) (Table 2). Adsorption isotherms for PSS and CMC (both sizes) were qualitatively of the Langmuir-type (Fig. 3), as has been reported for PSS adsorption on other types
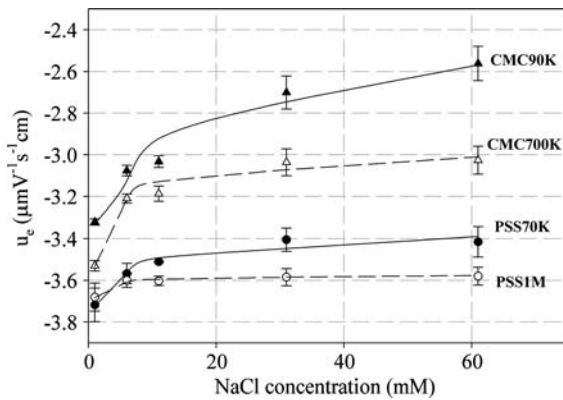

Fig. 4 Adsorption isotherms of PAP2.5K and PAP10K onto RNIP in 1 mM NaHCO$_3$. Curves are just connection between data points

of metal oxides (Blokhus and Djurhuus 2006) and for CMC on minerals (Wang and Somasundaran 2005). In contrast, PAP exhibited a distinct shoulder in the adsorption isotherm (Fig. 4) suggesting multilayer adsorption or self-association on the surface, similar to that reported for self-associating proteins and surfactants (Nylander 1998). Similar adsorption isotherms have been reported for PAP adsorption on hydroxyapatite (Guan et al. 2003).

Characteristics of the adsorbed polyelectrolyte layers

The magnitude and range of interparticle steric repulsions depends on the adsorbed polymer surface excess concentration and layer thickness. The EM of each polymer modified RNIP (at the maximum measured adsorbed mass) is plotted as a function of ionic strength in Fig. 5. Curves are the best fits of the average measured u_e to Eqs. 4–8. ζ-potential values for bare RNIP ranged from –38 to –28 mV for 1 to 61 mM NaCl, respectively. Best-fit curves for the average $u_e \pm \sigma$, or for PAP2.5K and PAP10K are not shown for clarity, but have similar quality fits as those shown. Regressed parameters including the layer thickness (d), the softness ($1/\lambda$), charge density (ZN/N_A) for each polymer from the Ohshima model fits are provided in Table 3. For each particle, the EM becomes less negative with increasing ionic strength due to compression of the electrical diffuse layer around the modified RNIP (Ohshima 1995a). While the mobility of bare, hard particles normally

Fig. 3 Adsorption isotherms of PSS70K, PSS1M, CMC90K, and CMC700K onto RNIP in 1 mM NaHCO$_3$. Curves are Langmuir fits of the data

803

Fig. 5 Electrophoretic mobility of the polyelectrolyte coated RNIP as a function of NaCl (mM) at pH 8.5 ± 0.1. The lines represent the best-fit theoretical curves obtained using Eqs. 4–8. The data and fits for PAP2.5K and PAP10K are not shown for clarity, but are of equal quality

converges to zero at high electrolyte concentration, the mobility of the polymer modified RNIP tend to reach a non-zero limiting value. The limiting value is different for each polymer modified RNIP, due to the different layer thickness (d), softness ($1/\lambda$), and charge density (ZN/N_A).

The measured layer thicknesses (d) for each polymer are consistent with expectations. Comparing the thicknesses of adsorbed PSS and CMC layers with comparable molecular weights, i.e. comparing PSS70K with CMC90K and PSS1M with CMC700K,

the thickness of adsorbed PSS is in general several folds greater than for CMC, yet the saturation surface excess concentrations for these polyelectrolytes are less than two fold different. This implies that adsorbed PSS chains are more extended than the CMC chains. This observation is consistent with a recent report that CMC adsorbed in a flat conformation on a talc surface (Wang and Somasundaran 2005). Furthermore, the CMC carboxyl groups can protonate to reduce the intra-layer charge density, and carboxyl groups are known to specifically adsorb to iron oxide surfaces (Chibowski and Wisniewska 2002); each factor would tend to favor a less extended chain conformation at the surface. In contrast, PSS is a strong polyelectrolyte that tends to have a constant degree of ionization in adsorbed layers (Biesheuvel 2004) which would favor an extended conformation.

In all cases, the thickness of the adsorbed layer increased with increasing molecular weight of the polyelectrolyte. Notably, the thickness of adsorbed PAP2.5K and PAP10K layers is as large as that of CMC700K even though PAP has a significantly lower molecular weight compared to CMC700K. The contour lengths of PAP2.5K and PAP10K are 10 and 39 nm, respectively, as roughly estimated from the molecular structure of PAP. Therefore, the relatively large estimated layer thicknesses of both PAP are a result of multilayer adsorption, as implied by the adsorption isotherm.

Table 3 Characteristics of the adsorbed polyelectrolyte layers at pH 8.5 ± 0.1 as estimated by Ohshima's soft particle analysis

Sample	ZN/N_A[a]	d[a]	$1/\lambda$[a]	$|\psi_{DON}|$[b]	$|\psi_0|$[b]	$\emptyset_P$	Stable fraction with respect to aggregation[c]	Stable fraction with respect to sedimentation[d]
	(mol/m³)	(nm)	(nm)	(mV)	(mV)	(10⁻³)	(% by vol.)	(% by mass)
PSS70K	0.17 ± 0.09	67 ± 7	41 ± 11	2.2 ± 1.1	1.1 ± 0.6	4.8	82	40
PSS1M	0.13 ± 0.08	198 ± 30	55 ± 20	1.7 ± 0.1	0.83 ± 0.2	0.3	35	10
CMC90K	0.35 ± 0.20	7.2 ± 3.2	9.2 ± 4.2	4.5 ± 2.5	19.7 ± 4.0	132.0	0	5
CMC700K	0.33 ± 0.07	40 ± 6.5	24 ± 0.6	4.2 ± 0.9	2.7 ± 0.1	15.4	52	20
PAP2.5K	0.37 ± 0.12	40 ± 12	24 ± 0.6	4.7 ± 1.5	2.9 ± 0.4	13.7	73	34
PAP10K	0.36 ± 0.21	44 ± 13	26 ± 5	4.6 ± 2.6	2.7 ± 1.0	10.7	82	32

[a] Errors are ± 1std as described in the experimental section

[b] The sign of ψ_{DON} and ψ_0 is negative

[c] The volume fraction of surface modified RNIP remaining in the size range from 10–80 nm over 1 h of aggregation in 1 mM NaCl and at pH = 8.5 ± 0.1

[d] The weight fraction of the surface modified RNIP remaining suspended after 7 h of sedimentation in 1 mM NaCl and at pH = 8.5 ± 0.1

For the measured EM, the ψ_0 values for polyelectrolyte-modified RNIP calculated from Ohshima's soft particle theory (Table 3) are significantly smaller ($\sim$ –3 mV) than the ζ-potential that would be calculated from Smoluchowski's formula ($\sim$ – 50 mV) which assumes a hard particle. This is typical for Ohshima's soft particle theory because the EM of soft particles is insensitive to the position of the slip plane so the hard particle assumption is invalid (Nakamura et al. 1992; Viota et al. 2004, 2005). The low electrical surface potential for polyelectrolyte-modified RNIP implies that electrostatic double layer repulsion does not play a major role in stabilizing polyelectrolyte-modified RNIP, and it is the electrosteric component that enhances the colloidal stability of polyelectrolyte-modified RNIP as discussed later.

Layer density, or effective volume fractions (ϕ_p), is another factor that can affect the steric component of polyelectrolyte-stabilized nanoparticles. Because the thicknesses of the adsorbed layers are significantly different for each polyelectrolyte and the surface excess concentrations are similar (~ 2 mg/m^2), the volume fraction of each polyelectrolyte adsorbed to the RNIP surface can be estimated (Eq. 9) from the measured average layer thickness and surface excess concentration, crudely approximating RNIP as a spherical particle of radius a.

$$\phi_p = 3 \frac{\Gamma_{max} a^2}{\rho_p [(d+a)^3 - a^3]} \tag{9}$$

ρ_p is the polyelectrolyte density. The calculated ϕ_p for each polyelectrolyte (Table 3) range from $\sim 5 \times 10^{-3}$ to 15×10^{-3}. The two outliers are CMC90K and PSS1M of which ϕ_p are 132×10^{-3} and 0.3×10^{-3} (i.e. the most and least dense layers in this study, respectively) are consistent with theoretical expectations. Charged homopolymers are normally adsorbed onto the surface in the train-loop-tail conformation (Fleer et al. 1993). Trains are favored at low degrees of chain polymerization while loops are favored with increasing degree of polymerization (Chodanowski and Stoll 2001), tending to increase the layer thickness. Therefore, CMC90K, which has a relatively low degree of polymerization and carboxylic functional groups that have a specific affinity for iron oxide should favor trains and thus assume a thin, dense conformation. Alternatively, PSS1M, has the highest degree of polymerization and a sulfonate charge unit that has no specific affinity to iron oxide, should form more loops and tails, and assume an extended configuration.

Intuitively, the softness parameter of the adsorbed layer should have an inverse relationship with layer densities. The softness parameter ($1/\lambda$) can be expressed as a function of frictional coefficient (γ) (Ohshima 1995a):

$$\frac{1}{\lambda} = \left(\frac{\eta}{\gamma} \right)^{1/2} \tag{10}$$

where

$$\gamma = 6\pi \eta a_p N_p \tag{11}$$

a_p is the radius of a resistance center corresponding to a polymer segment (Fig. 2c), and N_p is the volume density of polymer segments distributed in the adsorbed polyelectrolyte layer (Ohshima 1995a). Therefore, the higher the volume density of polymer segments in the layer, N_p, the lower the softness parameter. This is in good agreement with the trends observed in this study, i.e. CMC90K > CMC700K > PAP2.5K > PAP10K > PSS70K > PSS1M in terms of layer density (ϕ_p), or CMC90K < CMC700K $\approx$ PAP2.5K < PAP10K < PSS70K < PSS1M in terms of $1/\lambda$.

Effect of surface modification on RNIP aggregation

Adsorbed polyelectrolyte layers can provide electrosteric repulsions to enhance the NZVI dispersion stability with respect to aggregation and sedimentation. In this section, we qualitatively examine the effect of the adsorbed polyelectrolyte layers on the rate and extent of aggregation of bare and surface-modified RNIP. The effect of the adsorbed polyelectrolyte layer on sedimentation is discussed subsequently.

We previously demonstrated that bare RNIP rapidly aggregates in water at low ionic strength and low particle concentrations due to magnetic attractive forces between the particles (Phenrat et al. 2007). The distribution of hydrodynamic radii, R_H, for bare RNIP at the initial concentration of 5 mg/L is illustrated in Fig. 6. The distribution is initially
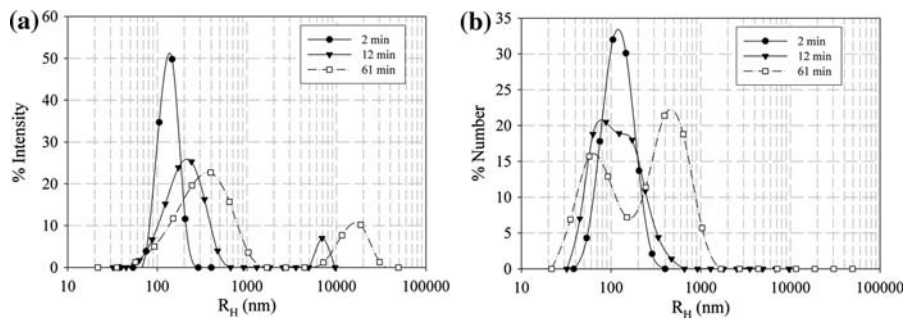
Fig. 6 Growth of the hydrodynamic radius, R$_H$, for bare RNIP at 5 mg/L. (**a**) Intensity-averaged distribution. (**b**) Number-averaged distribution

monomodal with an average R$_H$ of 136 nm after 2 min, indicating that the primary RNIP particles, which are 5 to 40 nm (average radius = 20 nm) (Nurmi et al. 2005), rapidly aggregate. After 12 min, large aggregates (>5,000 nm) appear and grow with time. The increase in R$_H$ for the smaller size mode appearing in the distribution corresponds to aggregation of RNIP to discrete micron-sized aggregates, while the increase in R$_H$ for the larger size mode appearing in the distribution corresponds to chain formation and gelation of those micron size aggregates as previously described (Phenrat et al. 2007). The intensity-averaged (Fig. 6a) and number-averaged (Fig. 6b) R$_H$ distribution showed similar behavior indicating that the majority of the bare RNIP population rapidly aggregates since the number-averaged particle size distribution is sensitive to aggregation only when a majority of the particle population aggregates.

For all surface modified RNIP, adsorbed polyelectrolyte layers affect the rate of aggregation and the fraction of the particle population that aggregates. The aggregating, unstabilized fraction is the fraction that has a continuously increasing particle size distribution over time. In contrast, the stabilized fraction is that with a relatively stable particle size distribution over time and a size range in good agreement with the individual particle size distribution as observed by TEM (R$_H$ = 5–40 nm) (Nurmi et al. 2005).

The measured R$_H$ for CMC90K modified RNIP is shown in Fig. 7. The average R$_H$ of the CMC90K modified RNIP was 166 nm after 1.5 min (Fig. 7a and b), similar to that observed for bare RNIP. This indicates that ~1 mg/m^2 of CMC90K adsorbed onto the surface at an estimated, average thickness layer of 7 nm is not sufficient to inhibit the aggregation of the major population of RNIP. However, the time it takes for aggregation to large gelled aggregates to form a bimodal distribution was longer (30 min), than for bare RNIP (12 min), and the stable size of individual aggregates (1st peak) that remain suspended becomes smaller (~262 nm) compared to bare RNIP (~360 nm). Thus, although the mass and the thickness of the adsorbed CMC90K layer is not sufficient to prevent aggregation, it slows down the rate and decreases the extent of aggregation.

In contrast, PSS70K modified RNIP did not form large aggregates. A significant fraction of the PSS70K modified RNIP (82% by volume) remains

Fig. 7 Growth of hydrodynamic radius, R$_H$, for CMC90K modified RNIP at 5 mg/L. (**a**) Intensity-averaged distribution. (**b**) Number-averaged distribution
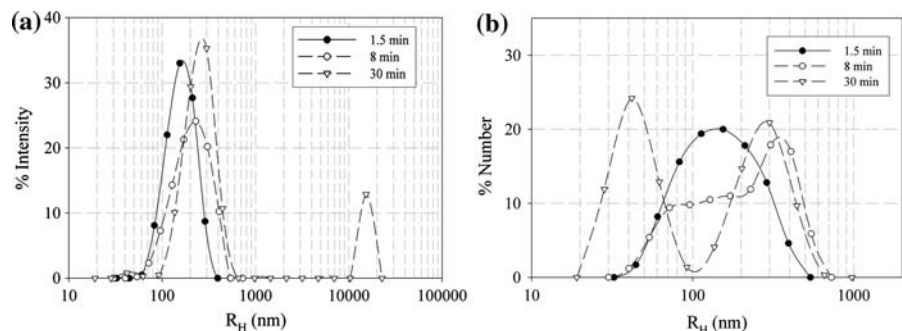
Fig. 8 Growth of hydrodynamic radius, R_H, for PSS70k modified RNIP at 5 mg/L, based on (**a**) intensity-averaged distribution and (**b**) number-averaged distribution
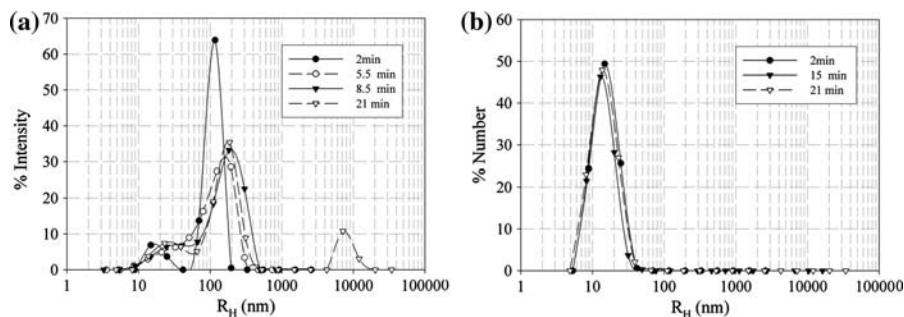
as individual RNIP with the R_H of 9 to 42 nm (Fig. 8a and b). For PSS70K, the number-averaged particle size distribution does not shift to the right with time, indicating that a majority of the particle population does not aggregate. The intensity-weighted size distribution becomes bimodal after 21 min, however, the fraction with R_H from 9 to 70 nm remains stable during the measurement. Thus, an adsorbed PSS 70K layer with the surface excess of ~ 2 mg/m^2 and the thickness of ~ 67 nm prevents a significant fraction of RNIP from rapid aggregation. CMC700K, PAP2.5K, and PAP10K modified RNIP showed the same behavior as the PSS70K modified RNIP (data not shown). For all modified RNIP, a fraction of particles rapidly aggregate to form a bimodal distribution, however, the fraction with R_H from 13 to 80 nm (52, 73, 82, and 82% by volume for the CMC700K-, PAP2.5K-, PAP10K-, and PSS70K-modified RNIP, respectively) remains rather stable over 60 min of aggregation study (Table 3). The volume fraction of RNIP stabilized by each modifier is qualitatively in good agreement with the mass adsorbed and the layer thickness of each modifier, suggesting that both high surface excess of modifier and an extended layer of sorbed polyelectrolytes are needed to stabilize RNIP.

Of the six polyelectrolytes evaluated, PSS1M modified RNIP was an outlier. Although the PSS1M modified RNIP has high surface excess (~ 2 mg/m^2) and a highly extended layer (~ 198 nm), only 35 vol% remained stable with R_H ranging from 13 to 110 nm (average $R_H = 30$ nm). A possible explanation is that PSS 1M does not provide steric stabilization due to inhomogenous surface coverage, a result of its large degree of polymerization and the small number (6) of polymer chains adsorbed to each particle compared to the other polyelectrolytes evaluated (Table 2). During a Brownian collision of two

PSS1M modified RNIP particles the PSS1M can move laterally, resulting in displacement coagulation (Napper 1983). This displacement coagulation is not expected for smaller polyelectrolytes such as PSS70K, CMC90K, PAP2.5K and PAP10K in this study because the number of the polyelectrolyte chains at the RNIP surface is quite high (Table 2); therefore, lateral movement is unlikely for these modifiers. As for CMC700K, although the average number of chains per RNIP particle (~ 9 chains) is lower than the smaller polyelectrolytes, the possibility of the lateral movement is lower than PSS1M because CMC has carboxylic groups which strongly anchor it to the Fe_3O_4 surface. This hypothesis is also supported by the small layer extension for CMC ($d = 40$ nm) compared to PSS1M ($d = 198$ nm).
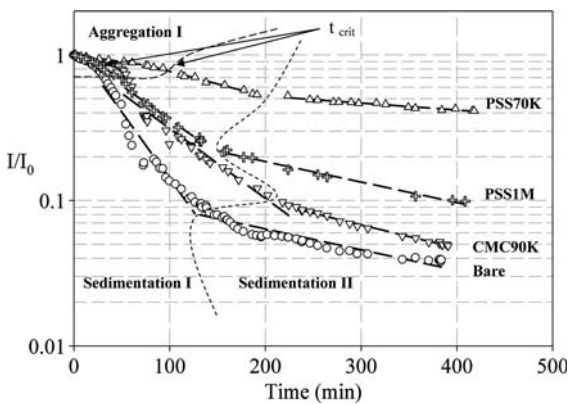
Effect of surface modification on RNIP sedimentation

A dispersion of nanoparticles can remain stable for very long time if the diffusion flux of nanoparticles, which is inversely proportional to the particle size and works in the opposite direction to the gravity, overcomes the sedimentation flux which is proportional to the square of the particle radius. When nanoparticles aggregate to micron-sized clusters, they tend to settle to the bottom of the container because the diffusion flux becomes smaller than the sedimentation flux. Thus, the sedimentation rate is a good indicator of colloidal stability of bare and polyelectrolyte-modified RNIP.

Aggregation, gelation, and sedimentation of aqueous bare RNIP dispersions were reported in our recent study (Phenrat et al. 2007). Here we examine the influence of the adsorbed polyelectrolyte layers on the sedimentation of aqueous dispersions of

surface modified RNIP. The sedimentation profile of bare RNIP dispersions consists of three regions: aggregation I, sedimentation I, and sedimentation II (Fig. 9). During aggregation I, the sedimentation rate is low while nanoparticles aggregate but largely remain suspended because they have not yet reached the critical size needed to sediment. At a time t_{crit}, the aggregates reach a critical size and begin to sediment rapidly (sedimentation I). Eventually, the sedimentation rate becomes low again, corresponding to the sedimentation of aggregates which did not form critical size chain-like clusters (Phenrat et al. 2007). For bare RNIP, only a small fraction of particles ($\sim$4%) remains suspended after 400 min, consistent with the DLS results indicating that a major fraction of the population of bare RNIP aggregates.

For modified RNIP, sedimentation follows the same pattern as the bare RNIP (Fig. 9), i.e. it consists of three different regions, however, important differences are notable and attributed to the presence of the adsorbed polyelectrolyte layers. First, the fraction of the surface modified RNIP remaining in the dispersion after 400 min is greater than that of the bare, i.e. $\sim$40, 34, 32, 20, 10, 5 wt% for PSS70K, PAP2.5K, PAP10K, CMC700K, PSS1M, CMC90K modified RNIP, respectively. The enhancement is because surface modification increases the population of RNIP particles which do not form critical sized aggregates and thus remain suspended. Second, the slope of the sedimentation curves (in the semi-log scale) in the sedimentation I region of the surface modified RNIP dispersions are smaller than that of

the bare (Fig. 9). The slope in this region is proportional to the average size of the aggregates formed (Phenrat et al. 2007). Therefore, the size of settling aggregates formed in the surface modified NZVI dispersions are smaller than those formed by bare RNIP. The fraction of surface modified RNIP stable at the end of Sedimentation II and the relative size of the settling aggregates are consistent with the volume fraction of surface modified RNIP remaining as individual particles as measured with DLS (Figs. 6–8). The stable fraction (wt%) with respect to sedimentation also correlates with the surface excess (mg/m^2) and thickness (nm) of the adsorbed polyelectrolyte layers (Fig. 10). The only outlier is PSS1M modified RNIP which is not considered in this correlation because unlike other modifiers, the PSS1M layer presumably fails to provide steric stabilization. Differences in the stable fractions are also apparent (visually) by comparing the color of the surface modified RNIP dispersions with the bare as is often reported (Bandyopadhyaya et al. 2002; Saleh et al. 2005). Even after several months of sedimentation, the PSS70K, PAP2.5K, and PAP10K modified RNIP dispersions at 0.8 g/L remain turbid and black while the bare RNIP dispersion at the same concentration becomes clear after 10 min. The lower

Fig. 9 Sedimentation curves for bare and surface modified RNIP dispersions (0.8 g/L) in 1 mM NaHCO$_3$ and pH = 8.5 ± 0.1 (semi-log)
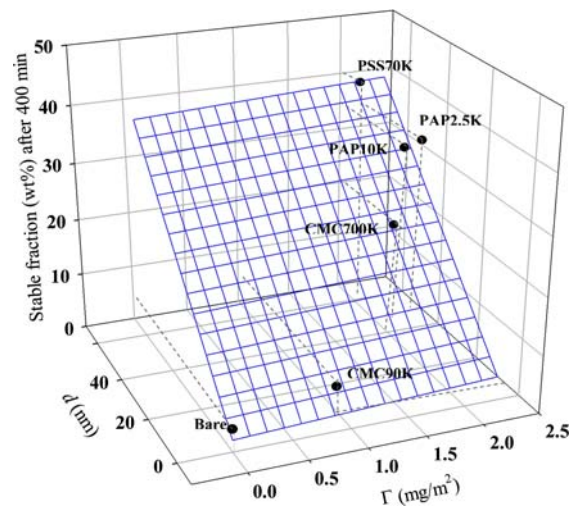
Fig. 10 Correlation between the stable fraction (wt%) observed in the Sedimentation II region and the measured surface excess (Γ, mg/m^2) and layer thickness (d, nm) of each adsorbed polyelectrolyte. The empirical relationship between the stable fraction (wt%) and Γ and d to form the plane is: stable fraction (wt%) = 2.05 + 0.91Γ(mg/m^2) + 0.58d(nm). The r^2 of the correlation is 0.92

aggregation and sedimentation rate of modified vs. bare particles implies that the probability of attachment during a collision between two surface modified RNIP particles, i.e. to overcome energy barrier, is lower that that of the bare.

It should be noted that aggregation and sedimentation kinetics are concentration-dependent, i.e. second order with respect to particle population (Evans and Wennerstrom 1999; Hiemenz and Rajagopalan 1997). However, the main objective of this study was to compare the efficacy of different polymeric surface modifiers. Thus, all other parameters including particle type and particle concentration were kept constant and the aggregation and sedimentation kinetics as a function of initial particle concentrations are not reported.

Extended DLVO theory to explain the influence of adsorbed polyelectrolyte layers on RNIP stabilization

The lower rate and extent of aggregation (Figs. 6–8) and increased unsedimented fraction (Figs. 9 and 10) of the surface modified RNIP compared to bare RNIP can be semi-quantitatively explained using DLVO theory extended to include magnetic and steric forces.

The time scale of colloidal dispersion stability is determined by the magnitude of the energy barrier between particles. According to classical DLVO theory, the major attractive energy is the van der Waals energy (V_{vdW}) while the major repulsive energy is electrostatic double layer interaction energy (V_{ES}) (Elimelech et al. 1995; Evans and Wennerstrom 1999; Hiemenz and Rajagopalan 1997). The V_{vdW} attractive energy between spherical particles can be expressed as (Elimelech et al. 1995; Hiemenz and Rajagopalan 1997)

$$\frac{V_{vdw}}{k_B T} = \frac{-A}{6 k_B T} \left[\frac{2a^2}{s(4a+s)} + \frac{2a^2}{(2a+s)^2} + \ln s \frac{(4a+s)}{(2a+s)^2} \right]$$
(12)

where A is the Hamaker constant, 10^{-19} J for RNIP (Phenrat et al. 2007), a is the radius of particles, k_B is Boltzmann's constant, and s is distance between the surfaces of two interacting particles. Electrostatic repulsion between two identical particles can be expressed as (Fritz et al. 2002)

$$\frac{V_{ES}}{k_B T} = \frac{2\pi \varepsilon_r \varepsilon_0}{k_B T} (a + \Delta) \psi_0^2 \ln[1 + e^{-\kappa(s-2\Delta)}]$$
(13)

where ε_r is the relative dielectric constant of the liquid, ε_0 is the permittivity of the vacuum, Δ is the thickness of the Stern layer, which in our case is taken to be the thickness of the adsorbed polyelectrolyte layer (d), ψ_0 is the surface potential of the particles, taken to be the potential at the outer edge of the adsorbed layer as determined by the Ohshima analysis, and κ is the Debye parameter.

RNIP behaves as a pseudo-single domain magnetic particle with a saturation magnetization M_s and has an intrinsic permanent magnetic dipole moment $\mu = (4\pi/3)a^3 M_s$ even in the absence of an applied magnetic field (Butter et al. 2003; McCurrie 1994; Phenrat et al. 2007). When particle dipoles are oriented in a head-to-tail configuration, the maximum magnetic attraction energy (V_M) can be expressed as (Gomez-Lopera et al. 2006; Phenrat et al. 2007; Viota et al. 2005)

$$\frac{V_M}{k_B T} = \frac{-8\pi \mu_0 M_s^2 a^3}{k_B T 9 (\frac{s}{a} + 2)^3}$$
(14)

where μ_0 is the magnetic permeability of the vacuum. Because RNIP has a Fe^0/Fe_3O_4 core-shell structure, the M_s of RNIP depends on the ratio of Fe^0/Fe_3O_4 content in the particles. An empirical relationship between Fe^0 (%) and M_s has been developed from magnetite particles ($\sim 0\%$ Fe^0), RNIP with various compositions (14.3% and 23.3% Fe^0) and elemental iron ($\sim 100\%$ Fe^0) (Fig. 11). The Fe^0 (wt%) of each surface modified RNIP was measured and used to estimate M_s as summarized in Table 4.

The potential energy of interaction for the bare RNIP that includes V_{vdW}, V_{ES}, and V_M is shown in Fig. 12a, where V_T is the sum of all contributing interactions. Considering only these forces, the magnetic attraction dominates the interaction energy, and there is no energy barrier to resist aggregation. This is in good agreement with the rapid aggregation observed for the major population of these bare particles (Phenrat et al. 2007).

However, for polyelectrolyte modified RNIP, two additional repulsive potentials must be considered: osmotic repulsion (V_{osm}) and elastic-steric repulsion (V_{elas}). Overlap of the polyelectrolyte layers on two approaching particles increases the local polymer
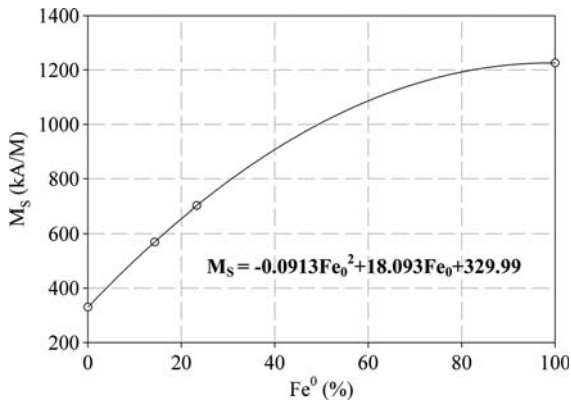
Fig. 11 Empirical relationship between the saturation magnetization, M_S, and the Fe^0 content of the particles. The curve was determined from from M_s measurements on magnetite, two RNIP particles having different Fe^0 contents, and on elemental iron (100% Fe^0)

segment concentration and thus increases the local osmotic pressure in the overlap region (V_{osm}). Any compression of the adsorbed polyelectrolyte layers below the thickness of the unperturbed layer (d) leads to a loss of entropy and gives rise to the elastic repulsion (V_{elas}) (Fritz et al. 2002). V_{osm} can be expressed as (Fritz et al. 2002)

$$\frac{V_{osm}}{k_B T} = 0 \qquad\qquad\qquad 2d \leq s$$

$$\frac{V_{osm}}{k_B T} = \frac{a4\pi}{\upsilon_1}\phi_p^2\left(\frac{1}{2}-\chi\right)\left(d-\frac{s}{2}\right)^2 \qquad d \leq s < 2d$$

$$\frac{V_{osm}}{k_B T} = \frac{a4\pi}{\upsilon_1}\phi_p^2\left(\frac{1}{2}-\chi\right)d^2\left(\frac{s}{2d}-\frac{1}{4}-\ln\left(\frac{s}{d}\right)\right) \quad s<d$$

$$(15)$$

Table 4 Measured Fe^0 of each surface modified RNIP and the estimated saturation magnetization, M_s

Modifier	Fe^0 content (%)	Estimated M_S (kA/M)[a]
None	26 ± 0.5	741 ± 10
PSS70K	15 ± 0.0	589 ± 1
PSS1M	15 ± 0.7	576 ± 15
CMC700K	29 ± 1.4	779 ± 25
CMC90K	24 ± 0.3	706 ± 5
PAP10K	25 ± 1.3	727 ± 24
PAP2.5K	24 ± 0.6	712 ± 11

[a] Estimated using the empirical relationship between Fe^0 and M_s according to Fig. 11

where χ is the Flory-Huggins solvency parameter which is assumed to be 0.45 for all polyelectrolytes in this study, ϕ_p is the calculated volume fraction of polymer within the brush layer (Table 3), d is the thickness of the brush, and υ_1 is the volume of a solvent molecule.

V_{elas} can be expressed as (Fritz et al. 2002):

$$\frac{V_{elas}}{k_B T} = 0 \quad d \leq s$$

$$\frac{V_{elas}}{k_B T} = \left(\frac{2\pi a}{M_w}\phi_p d^2 \rho_p\right)\left(\frac{s}{d}\ln\left(\frac{s}{d}\left(\frac{3-s/d}{2}\right)^2\right)\right) \qquad (16)$$
$$-6\ln\left(\frac{3-s/d}{2}\right)+3\left(1+\frac{s}{d}\right)^2\right) \quad d > s$$

where M_W is the molecular weight of the polyelectrolyte, and ρ_p is its density. Assuming an average particle radius a = 20 nm, the potential energy of interaction for the PSS70K, CMC90K, and PAP2.5K modified RNIP that includes V_{vdW}, V_{ES}, V_M, V_{osm}, and V_{elas} is shown in Fig. 12b, c, and d, respectively. For separation distances beyond 2d, the long-ranged attractive magnetic force is still dominant and results in the net attractive potential. However, when the coated particles approach one another to a distance less than 2d, there is a large energy barrier due to the adsorbed layer. As shown in the potential energy diagram for a = 20 nm, the steric forces cause the secondary minimum (potential well) of –4.25, –157, and –14.6 $k_B T$ at 123, 15, and 80 nm for PSS70K, CMC90K, and PAP2.5K modified RNIP, respectively. Thus, according to these diagrams, the PSS70K, CMC90K, and PAP2.5K modified particles should form loose aggregates (in the secondary minimum) with a separation distance of 123, 15, and 80 nm, respectively rather than dense aggregates with no separation as in the case of bare RNIP (Phenrat et al. 2007).

Considering Eqs. 12–16, the calculated potentials are a function of the radius of particles, a, especially long-range attractive interactions such as magnetic attraction which depends on the particle radius to the sixth power. Because RNIP is polydisperse with radii ranging from 5 to 40 nm (average radius = 20 nm) (Nurmi et al. 2005), the potentials for a pair of particles with different radii can vary significantly and can qualitatively explain why these polyelectrolytes can stabilize just some portion of RNIP. The depth of the secondary minimum (potential well)

Fig. 12 Potential energy of interaction for a pair of RNIP particles having an average radius of 20 nm at 1 mM NaCl background electrolyte and pH 8.5. (**a**) bare RNIP, (**b**) PSS70K modified RNIP, (**c**) CMC90K modified RNIP, and (**d**) PAP2.5K modified RNIP
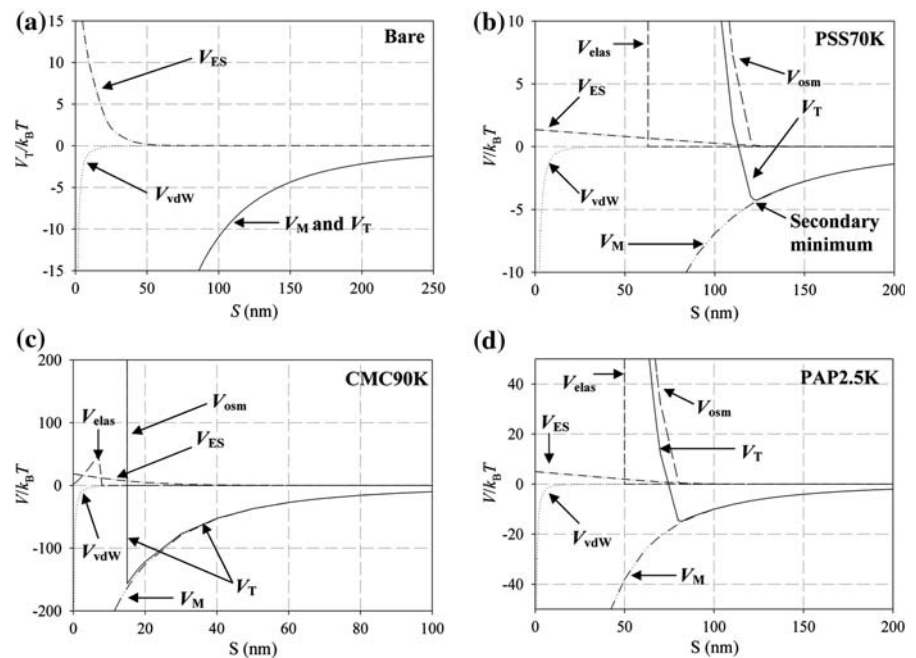
between two identical particles is plotted as a function of their radius a (nm) in Fig. 13. For a distribution of radii from 5 to 40 nm, the value of the potential well varies by several orders of magnitude, indicating the importance of particle size on their aggregation potential. Weak aggregation (or i.e. coagulation) is expected if the depth of the secondary minimum is just greater that the thermal energy, $1.5k_BT$ (Napper 1983). For a weaker attraction, reversible aggregation is expected (Napper 1983; Viota et al. 2005). As shown in Fig. 13, a pair of particles with radii smaller than ~ 8, 12, 14, and 17 nm for CMC90K, CMC700K, PAP2.5K, and PSS70K modified RNIP provides repulsive forces between particles and is theoretically expected to resist aggregation. This is qualitatively in good agreement with the experimental results which observe stable fractions in these surface modified RNIP with respect to aggregation and sedimentation (Figs. 6–9). Qualitatively, the extent of the stable volume and mass (%) observed in the aggregation and sedimentation study agrees with the trends estimated by DLVO for each type of polyelectrolyte modified RNIP, i.e. PSS70K > PAP2.5K $\sim$ PAP10K > CMC700K > CMC90K. DLVO also qualitatively confirms the observation that none of the polyelectrolytes can prevent aggregation and sedimentation of the larger RNIP particles present in
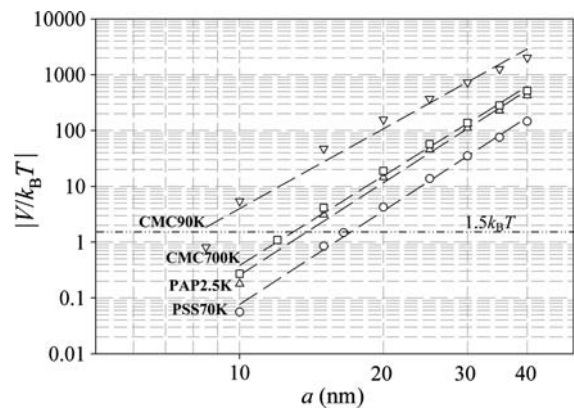
Fig. 13 The calculated absolute value of the secondary minimum (potential well) interaction energy predicted for the collision of two identical surface modified RNIP with radius a (nm)

the polydisperse slurry. For these larger particles, the magnetic attractive force outweighs the steric forces at $2d$, yielding a secondary minimum with a potential energy much greater than $1.5k_BT$ and subsequent aggregation. Of course, large particles could still attract some smaller particles, but sedimentation of these larger aggregates before they collide with many smaller particles may leave a significant fraction of the smallest particles suspended.

Applying this simplified calculation to PSS1M modified RNIP predicts the largest stable fraction. This contrasts to both aggregation and sedimentation results which reveal that only relatively small fraction remains stable. This disagreement can be explained by non-thermodynamically limited steric stabilization (Napper 1983) as noted above. For Eqs. 15 and 16 to be valid, the lateral movement of adsorbed polyelectrolytes onto RNIP surface is not allowed.

Conclusions

This study investigated the stabilization of polydisperse nanoscale zerovalent iron (NZVI) particles (5–40 nm in radius) using commercially available anionic polyelectrolytes, PSS, CMC, and PAP. The maximum surface excess concentration for each of these polyelectrolytes adsorbed on NZVI was $\sim$1–2 mg/m^2. The layer thicknesses estimated using electrophoretic mobility and Ohshima's soft particle analysis are $\sim$7 nm for CMC90K, $\sim$40 nm for CMC90K, PAP2.5K, and PAP10K, $\sim$67 nm for PSS70K, and $\sim$198 nm for PSS1M. The stable fractions with respect to both aggregation and sedimentation correlate with the adsorbed mass and layer thickness, indicating that both of these properties must be considered when predicting the stability of polyelectrolyte-stabilized nanoparticles. A fraction of the polydisperse particles used in this study could not be stabilized regardless of the modifier used and rapidly aggregated to micron sized fractal aggregates as observed for bare NZVI. This sedimented fraction is attributed to the larger particles present in the polydisperse NZVI suspension as the magnetic attractive forces increase as r^6. According to the aggregation and sedimentation measurements, PSS70K, PAP2.5K, and PAP10K perform best in NZVI stabilization, i.e. 40, 32, 34 wt% of the PSS70K, PAP2.5K, and PAP10K modified NZVI remain suspended for more than several months.

Appendix

Effects of particle polydispersity on Ohshima's soft particle analysis

Equation 4 consists of three terms: the first term is a weighted average of the Donnan potential (ψ_{DON}) and the surface potential (ψ_0), the second term is the ratio of the electric force acting on the layer fixed charges ($EZeN$) and the frictional force (γu), and the third term is due to the zeta potential (ζ) of the bare particle (Ohshima 1995a). The first term has the correction factor $f(d/a)$ that accounts for alteration of an applied electric field acting on the polyelectrolyte layer due to the presence of a particle core (Ohshima 1994). This term is a function of the radius of bare particles a and the layer thickness (Eq. 7). For polydisperse colloidal particles with a range of radii $a_{min} - a_{max}$ and an average radius a_{ave}, and assuming that the layer thickness d is the same for all particles in this size range, using a_{ave} as a representative of the entire particle population in Eq. 4 may lead to error in estimating the layer parameters because each a in the population of $a_{min} - a_{max}$ has a different degree of applied electric field alteration and, thus, a different $f(d/a)$.

Further analysis of $f(d/a)$ can be done to show that there are two obvious cases where particle polydispersity does not affect the sensitivity of the calculated adsorbed polyelectrolyte layer properties. Figure A1a shows $f(d/a)$ as a function of d/a. $f(d/a)$ consists of three regions. Regions 1 and 3 represent the cases of a very thin ($d \ll a$) and a very thick ($d \gg a$) adsorbed polyelectrolyte layer, respectively, with respect to radius of the particle. The $f(d/a)$ of both regions become constant, 1 and 2/3, respectively, with respect to d/a. In region 3, d is much larger than a; the applied electric field acting on the polyelectrolyte layer is not significantly altered by the presence of the core a. Therefore, $f(d/a)$ becomes a constant, 2/3, which is similar to the case of a spherical polyelectrolyte without a core (Ohshima 1994). In contrast, in region 1, d is much smaller than a; the applied electric field acting on the polyelectrolyte layer becomes so distorted that it can have only its tangential component near the particle core (Ohshima 1995a). The value of this distorted field is about 3/2 times larger than the undisturbed field in the absence of the particle core,
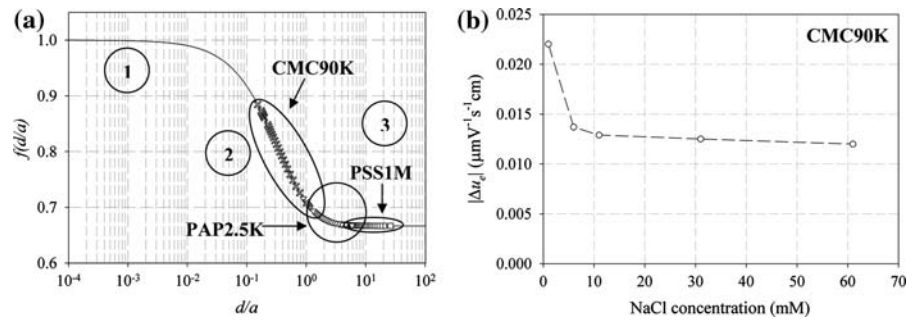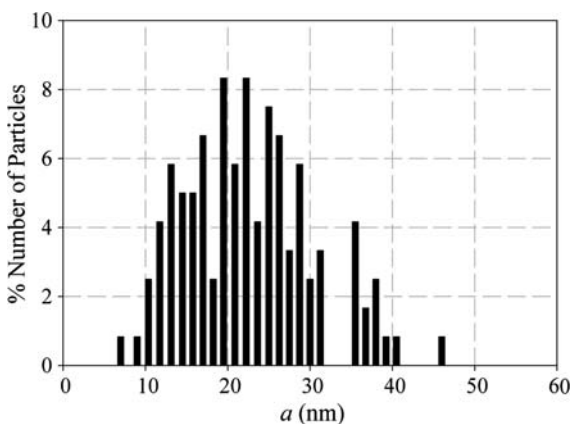
i.e. $f(d/a)$ in region 1 is $\sim 3/2$ times of $f(d/a)$ in region 3 or ~ 1. For this reason, in region 1 and 3, $f(d/a)$ becomes a constant, and Eq. 4 becomes independent of a. Consequently, particle polydispersity does not affect the sensitivity of the calculated adsorbed polyelectrolyte layer properties using Ohshima's soft particle theory if the properties of soft polydisperse particles fall into those two extreme regions. However, in region 2, the intermediate case, $f(d/a)$ varies from 1 to 2/3, and the calculated layer properties may be sensitive to the particle polydispersity.

Figure A2 illustrates the particle size distribution of bare RNIP determined from transmission electron microscope (TEM) images. d/a values calculated from the RNIP particle size distribution and the calculated d for polyelectrolyte-modified RNIP in this study reveal that PSS70K-, PSS1M-, CMC700K-, PAP2.5K-, and PAP10K-modified RNIP all fall into region 3 (Fig. A1a shows only PSS1M- and

Fig. A2 Particle size distribution of RNIP obtained form TEM images

PAP2.5K-modified RNIP). Therefore, RNIP polydispersity should not affect the calculated layer properties of these polyelectrolyte modified RNIP. In contrast, CMC90K-modified RNIP lies in region 2 and the calculated layer properties using Ohshima's soft particle theory may be affected by the RNIP polydispersity.

We theoretically evaluated (1) if RNIP polydispersity affects the appropriateness of using a_{ave} in Eq. 4 to represent the particle population for CMC90K-modified RNIP, and (2) if particle polydispersity affects the sensitivity of the calculated adsorbed CMC90K layer properties. To evaluate the former, the difference between u_e calculated using only a_{ave} ($u_{e\text{-}ave}$) and the average of u_e calculated from u_e determined for each particle diameter in the entire particle size distribution ($u_{e\text{-}poly}^{ave}$) was determined for the layer properties for CMC90K-modified RNIP (Table 3). The distribution of $u_{e\text{-}poly}$ is essentially a normal distribution with a mean of $u_{e\text{-}poly}^{ave}$ (Eq. A1, Fig. A3a). The difference between $u_{e\text{-}ave}$ and $u_{e\text{-}poly}^{ave}$ was attributed to the effect of particle polydispersity (Fig. A1b).

$$\%number(u_e, u_{e-ave}, \sigma_{ue})$$
$$= \frac{1}{\sigma_{ue}\sqrt{2\pi}}\exp\left(-\frac{(u_e - u_{e-poly}^{ave})^2}{2\sigma_{ue}^2}\right) \quad (A1)$$

To determine the sensitivity of the calculated layer properties, $d_{poly}, 1/\lambda_{poly}$, and N_{poly} to polydispersity, $u_{e\text{-}poly}^{ave}$ values at various ionic strengths (1 to 61 mM) were fit using Eqs. 4–8 and a least-squares fitting protocol. These calculated properties, which account for polydispersity, are then compared to the properties determined from ue-ave alone (Table 3). The difference between these two sets of parameters (Δd, $\Delta 1/\lambda$, and ΔN) is attributed to particle polydispersity effect. As shown Fig. A3a, particle polydispersity
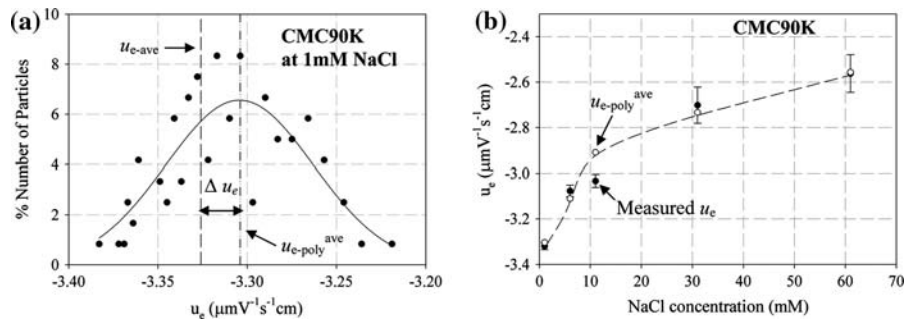
Fig. A3 (a) Effect of particle polydispersity on the difference between $u_{e\text{-}ave}$ and $u_{e\text{-}poly}^{ave}$ (Δu_e) for CMC90K-modified RNIP in 1 mM NaCl. The filled circles represent $u_{e\text{-}poly}$ theoretically generated by from the layer characteristics of CMC90K

does indeed affect $u_{e\text{-}poly}^{ave}$ of CMC90K-modified RNIP because their d/a are in region 2. However, the effect is small and the best fit curve for both cases are the same (Fig. A3b), yielding the same layer properties. Thus, the calculated layer properties for CMC90K-modified RNIP are indeed insensitive to polydispersity, i.e. Δd, $\Delta l/\lambda$, and $\Delta N = 0$.

References

Allain C, Cloitre M (1993) The effects of gravity on the aggregation and the gelation of colloids. Adv Colloid Interface Sci 46:129–138

Bandyopadhyaya R, Nativ-Roth E, Regev O, Yerushalmi-Rozen R (2002) Stabilization of individual carbon nanotubes in aqueous solutions. Nano Lett 2(1):25–28

Biesheuvel PM (2004) Ionizable polyelectrolyte brushes: brush height and electrosteric interaction. J Colloid Interface Sci 275(1):97–106

Blokhus AM, Djurhuus K (2006) Adsorption of poly(styrene sulfonate) of different molecular weights on alpha-alumina: effect of added sodium dodecyl sulfate. J Colloid Interface Sci 296:64–70

Box GEP, Hunter WG, Hunter JS (1978) Statistics for experimenters: an introduction to design, data analysis, and model building. Wiley-Interscience, New York

Butter K, Bomans PH, Frederik PM, Vroege GJ, Philipse AP (2003) Direct observation of dipolar chains in ferrofluids in zero field using cryogenic electron microscopy. J Phys Condens Matter 15:S1451–S1470

Chen K-L, Elimelech M (2006) Aggregation and deposition kinetics of fullerene (C-60) nanoparticles. Langmuir 22(26):10994–11001

Chibowski S, Wisniewska M (2002) Study of electrokinetic properties and structure of adsorbed layers of polyacrylic acid and polyacrylamide at Fe_2O_3–polymer solution interface. Colloids Surf A 208(1–3):131–145

Chodanowski P, Stoll S (2001) Polyelectrolyte adsorption on charged particles in the Debye-Hückel approximation. A Monte Carlo approach. Macromolecules 34(7):2320–2328

(Table 3) and particle size distribution of RNIP (Fig. A2). The curve is the fit of the data according to Eq. A1. (b) Measured u_e and $u_{e\text{-}poly}^{ave}$ as a function of ionic strengths and their least-squares fit of Eq. 4

Dunphy Guzman KA, Finnegan MP, Banfield JF (2006) Influence of surface potential on aggregation and transport of titania nanoparticles. Environ Sci Technol 40(24): 7688–7693

Duro R, Souto C, Gómez-Amoza JL, Martínez-Pacheco R, Concheiro A (1999) Interfacial adsorption of polymers and surfactants: implications for the properties of disperse systems of pharmaceutical interest. Drug Dev Ind Pharm 25(7):817–829

Elimelech M, Gregory J, Jia X, Williams R (1995) Particle deposition and aggregation: measurement, modeling, and simulation. Butterworth-Heinemann, Boston

Elliott DW, Zhang W-X (2001) Field assessment of nanoscale bimetallic particles for groundwater treatment. Environ Sci Technol 35:4922–4926

Evans DF, Wennerstrom H (1999) The colloidal domain; where physics, chemistry, biology, and technology meet. Wiley-VCH, New York

Fleer GJ, Cohen Stuart MA, Scheutjens JMHM, Cosgrove T, Vincent B (1993) Polymers at interfaces. Chapman & Hall, London

Fritz G, Schadler V, Willenbacher N, Wagner NJ (2002) Electrosteric stabilizatoin of colloidal dispersions. Langmuir 18:6381–6390

Goddard ED, Vincent B (1984) Polymer adsorption and dispersion stability. ACS, Washington

Gomez-Lopera SA, Arias JL, Gallardo V, Delgado AV (2006) Colloidal stability of magnetite/poly(lactic acid) core/shell nanoparticles. Langmuir 22(6):2816–2821

Guan YH, Lath DL, de Graaf T, Lilley THAHB (2003) Moderation of oral bacterial adhesion on saliva-coated hydroxyapatite by polyaspartate. J Appl Microbiol 94:456–461

Henn KW, Waddill DW (2006) Utilization of nanoscale zerovalent iron for source remediation—A case study. Remediat J 16:57–77

Hiemenz P, Rajagopalan R (1997) Principles of colloid and surface chemistry. CRC, New York

Holmberg K, Jonsson B, Kronberg B, Lindman B (2003) Surfactants and polymers in aqueous solution. John Wiley&Sons, Ltd., West Sussex

Kanel SR, Nepal D, Manning B, Choi H (2007) Transport of surface-modified iron nanoparticle in porous media and

application to arsenic(III) remediation. J Nanopart Res 9(5):725–735

Kim B, Sigmund WM (2004) Functionalized multiwall carbon nanotube/gold nanoparticle composites. Langmuir 20(19):8239–8242

Liu Y, Lowry GV (2006) Effect of particle age (Fe^0 content) and solution pH on NZVI reactivity: H$_2$ evolution and TCE dechlorination. Environ Sci Technol 40(19):6085–6090

Liu Y, Majetich SA, Tilton RD, Sholl DS, Lowry GV (2005) TCE dechlorination rates, pathways, and efficiency of nanoscale iron particles with different properties. Environ Sci Technol 39(5):1338–1345

Mays DC, Hunt JR (2005) Hydrodynamic aspects of particle clogging in porous media. Environ Sci Technol 39(2):577–584

McCurrie RA (1994) Ferromagnetic materials: structure and properties. Academic Press, London

Nakamura M, Ohshima H, Kondo T (1992) Electrophoretic behavior of antigen- and antibody-carrying latex particles. J Colloid Interface Sci 149(1):241–246

Napper DH (1983) Polymeric stabilization of colloidal dispersions. Academic Press, New York

Nurmi JT, Tratnyek PG, Sarathy V, Baer DR, Amonette JE, Pecher K, Wang C, Linehan JC, Matson DW, Penn RL, Driessen MD (2005) Characterization and properties of metallic iron nanoparticles: spectroscopy, electrochemistry, and kinetics. Environ Sci Technol 39(5):1221–1230

Nylander T (1998) Protein adsorption in relation to solution association and aggregation. In: Malmsten M (eds) Biopolymer at interfaces. Marcel Dekker, New York, pp 409–452

Ohshima H (1994) Electrophoretic mobility of soft particles. J Colloid Interface Sci 163:474–483

Ohshima H (1995a) Electrophoresis of soft particles. Adv Colloid Interface Sci 62:189–235

Ohshima H (1995b) Electrophoretic mobility of soft particles. Colloids Surf A 103:249–255

Ohshima H, Nakamura M, Kondo T (1992) Electrophoretic mobility of colloidal particles coated with a layer of adsorbed polymers. Colloid Polym Sci 270:873–877

Phenrat T, Saleh N, Sirk K, Tilton RD, Lowry GV (2007) Aggregation and sedimentation of aqueous nanoscale zerovalent iron dispersions. Environ Sci Technol 41(1):284–290

Ponder SM, Darab JG, Mallouk TE (2000) Remediation of Cr(VI) and Pb(II) aqueous solutions using supported, nanoscale zero-valent iron. Environ Sci Technol 34:2564–2569

Ramos-Tejada MM, Ontiveros A, Viota JL, Durán JDG (2003) Interfacial and rheological properties of humic acid/hematite suspensions. J Colloid Interface Sci 268(1):85–95

Romero-Cano MS, Martín-Rodríguez A, de las Nieves FJ (2001) Electrosteric stabilization of polymer colloids with different functionality. Langmuir 17:3505–3511

Rosenweig RE (1985) Ferrohydrodynamics. Cambridge University Press, New York

Saleh N, Phenrat T, Sirk K, Dufour B, Ok J, Sarbu T, Matyjaszewski K, Tilton RD, Lowry GV (2005) Adsorbed triblock copolymers deliver reactive iron nanoparticles to the oil/water interface. Nano Lett 5(12):2489–2494

Saleh N, Sirk K, Liu Y, Phenrat T, Dufour B, Matyjaszewski K, Tilton RD, Lowry GV (2007) Surface modifications enhance nanoiron transport and NAPL targeting in saturated porous media. Environ Eng Sci 24(1):45–57

Sato T, Ruch R (1980) Stabilization of colloidal dispersions by polymer. Adsorption Marcel Dekker, New York

Singh BP, Menchavez R, Takai C, Fuji M, Takahashi M (2005) Stability of dispersions of colloidal alumina particles in aqueous suspensions. J Colloid Interface Sci 291(1):181–186

Strenge K (1993) Structure formation in disperse systems In: Dobias B (ed) Coagulation and flocculation: theory and applications. Marcel Dekker, New York

Tsuneda S, Aikawa H, Hayashi H, Hirata A (2004) Significance of cell electrokinetic properties determined by soft-particle analysis in bacterial adhesion onto a solid surface. J Colloid Interface Sci 279:410–417

Viota JL, de Vicente J, Ramos-Tejada MM, Durán JDG (2004) Electrical double layer and rheological properties of yttria-stabilized zirconia suspensions in solutions of high molecular weight polyacrylic acid polymers. Rheol Acta 43:645–656

Viota JL, de Vicente J, Duran JDG, Delgado AV (2005) Stabilization of magnetorheological suspensions by polyacrylic acid polymers. J Colloid Interface Sci 284:527–541

Wang J, Somasundaran P (2005) Adsorption and conformation of carboxymethyl cellulose at solid-liquid interfaces using spectroscopic, AFM and allied techniques. J Colloid Interface Sci 291:75–83

Wiesner MR, Lowry GV, Alvarez P, Dionysiou D, Biswas P (2006) Assessing the risks of manufactured nanomaterials. Environ Sci Technol A-Pages 40(14):4336–4337

Williams DN, Gold KA, Pulliam Holoman TR, Ehrman SH, Wilson OC (2006) Surface modification of magnetic nanoparticles using gum arabic. J Nanopart Res 8(5):749–753

Wu L, Shamsuzzoha M, Ritchie SMC (2005) Preparation of cellulose acetate supported zero-valent iron nanoparticles for the dechlorination of trichloroethylene in water. J Nanopart Res 7:469–476

Xu J, Dozier A, Bhattacharyya D (2005) Synthesis of nano-scale bimetallic particles in polyelectrolyte membrane matrix for reductive transformation of halogenated organic compounds. J Nanopart Res 7:449–467

Zhang W (2003) Nanoscale iron particles for environmental remediation: an overview. J Nanopart Res 5:323–332